Supplementary Information for

Early leaf senescence reveals drought stress thresholds and mortality risk across temperate forests

Pia Labenski[1*], Allan Buras[2], Rüdiger Grote[1], Martin Thurner[1], Nadine K. Ruehr[1]

[1]Institute of Meteorology and Climate Research – Atmospheric Environmental Research (IMKIFU), Karlsruhe Institute of Technology (KIT), Garmisch-Partenkirchen, Germany

[2]Technical University of Munich (TUM), Land-Surface-Atmosphere Interactions, Freising, Germany

*corresponding author: pia.labenski@kit.edu

Field observations of senescence onset (ICP Forests) and correlation with satellite-based estimates

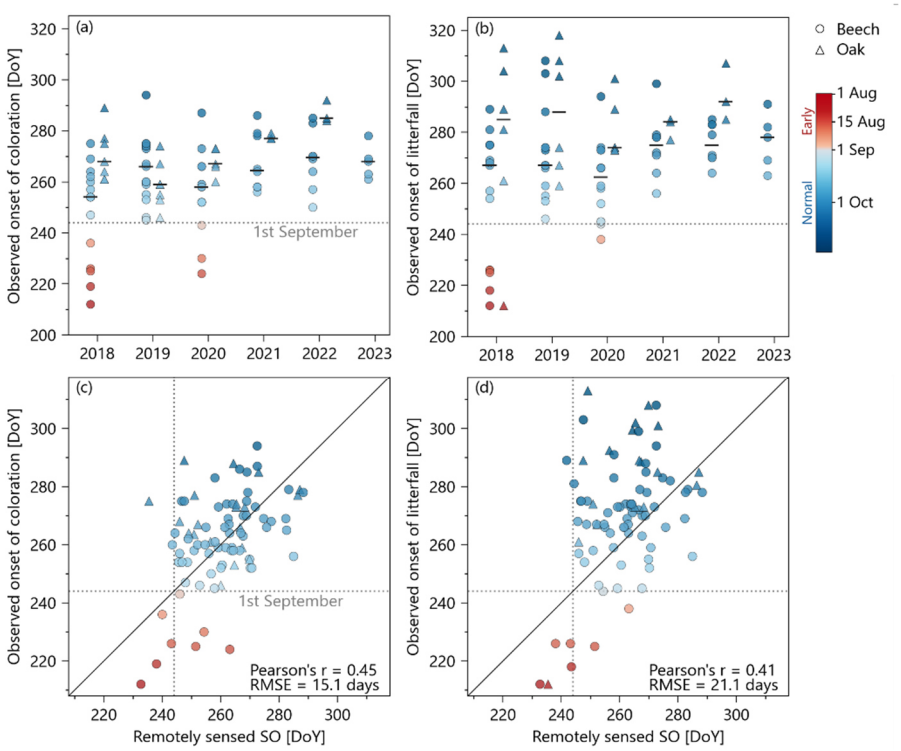

Figure S1: Onset of leaf senescence in beech and oak forests in Germany (2018-2023) derived from ground-based observations and remote sensing. Ground data are from ICP Forests Level II plots (http://icp-forests.net) and include recordings of a) 'infrequent or slight' coloration (1-33% of the canopy affected), and b) 'infrequent or slight' litterfall. Note that the number of observed plots varied annually (n=5-16 for beech, n=3-7 for oak). Circles and triangles represent individual beech and oak observations, horizontal black lines show annual medians. Relationships with remotely-sensed senescence onset (SO) are shown as c) coloration observations vs. SO derived from Sentinel-2 Normalized Difference Red-Edge Index (NDRE) time series using a threshold of 80% of the seasonal amplitude and d) litterfall observations vs. the same NDRE-based SO. Note that the remotely sensed SO was here averaged over an area of 40x40 km around the ICP Forests plots, therefore representing a regionalized senescence signal.

Field-satellite comparison at different aggregation scales for infrequent/slight canopy coloration and litterfall

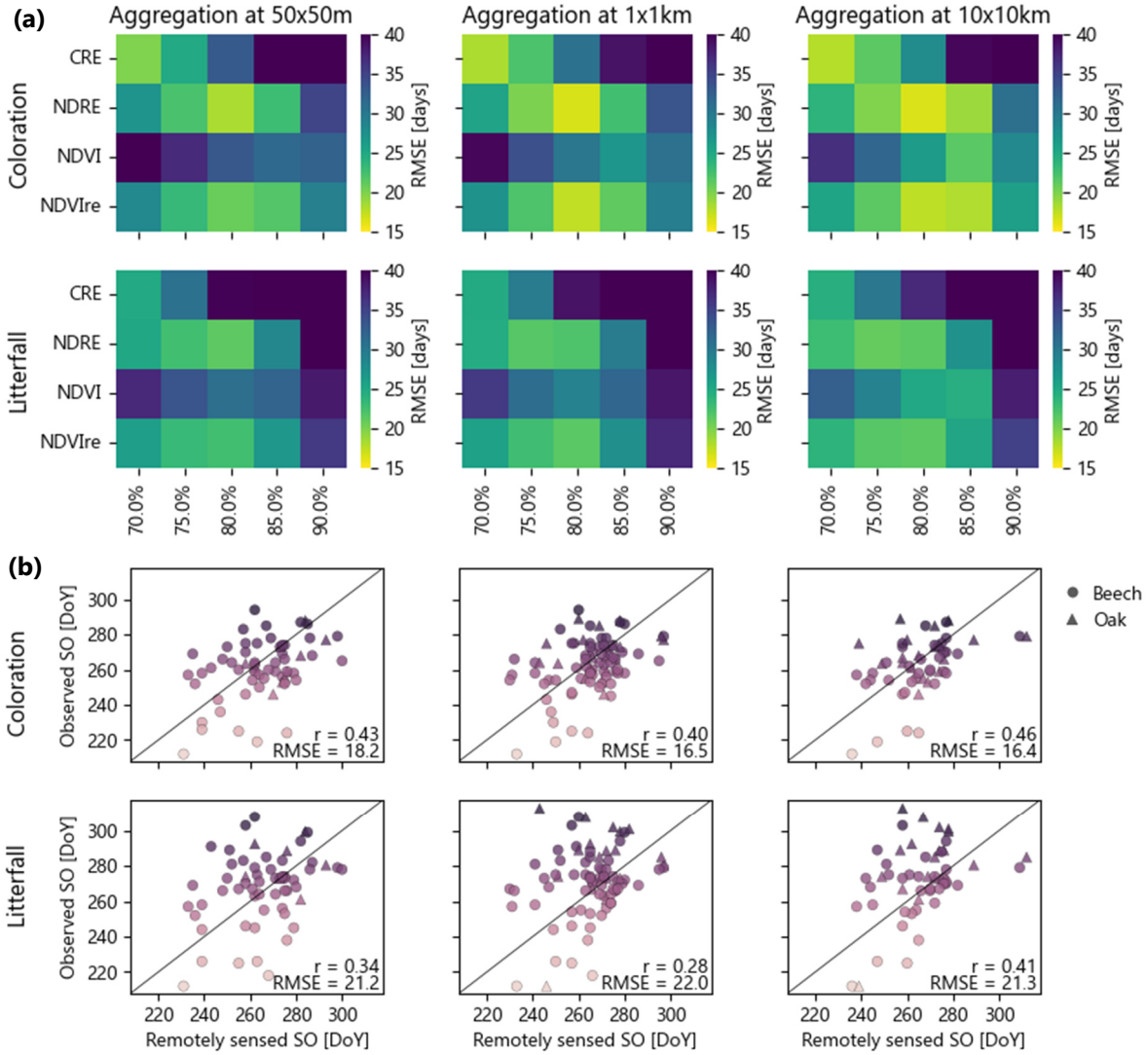

Figure S2: (a) RMSE between field-observed (ICP Forests category 'infrequent or slight', 1-33% of canopy affected) and remotely sensed senescence onset (SO) across different vegetation indices and amplitude thresholds. The Normalized Difference Red-Edge Index (NDRE) at the 80% amplitude threshold provides the best agreement for both coloration and litterfall onset across different aggregation resolutions. (b) shows the correlation between field-observed coloration and litterfall onset dates and the remotely sensed SO derived from NDRE_80%.

Field-satellite comparison at different aggregation scales for common/moderate canopy coloration and litterfall

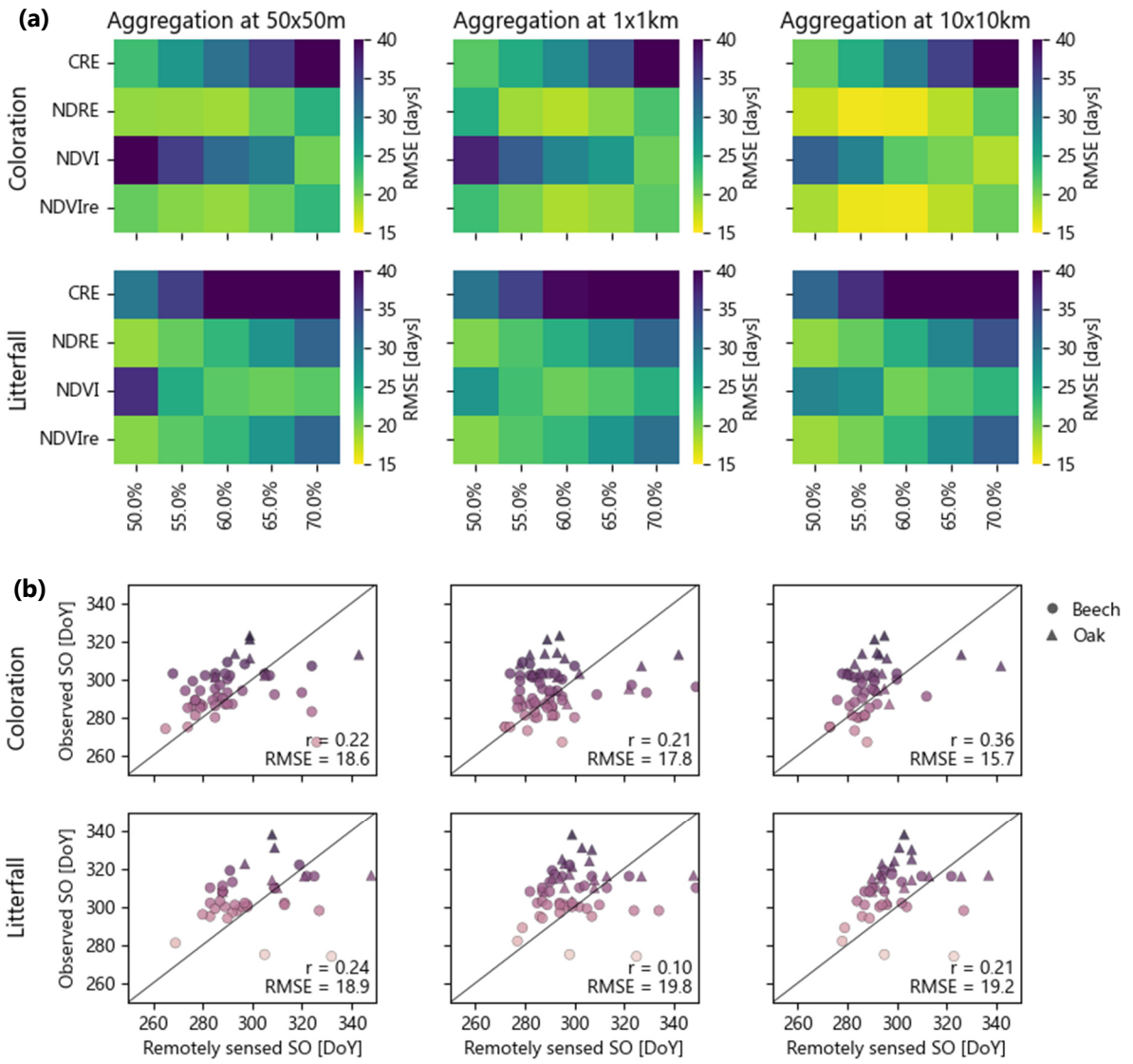

Figure S3: (a) RMSE between field-observed (category 'common or moderate', 33-66% of canopy affected) and remotely sensed senescence onset (SO) across different vegetation indices (VIs) and amplitude thresholds. The Normalized Difference Red-Edge Index (NDRE) at the 60% amplitude threshold provides the best agreement for coloration, while NDRE at 50% best agrees with litterfall onset across different aggregation resolutions. (b) shows the correlation between field-observed coloration and litterfall onset dates and the remotely sensed SO derived from the respective best-performing VI-threshold combination.

Supplementary Note 1: **Discussion of satellite-derived senescence onset**

Our analysis showed moderate agreement between satellite-derived senescence onset (SO) and field observations of coloration and litterfall, with remote sensing tending to underestimate early senescence. Discrepancies between the two datasets are expected, given their respective sources of uncertainty and different observational perspectives. The accuracy of satellite-based SO is influenced by noise from cloud contamination and atmospheric effects, as well as by the filtering, interpolation, and smoothing steps required for phenology extraction. Understory and admixed tree species may additionally alter the signal. Field observations are similarly subject to uncertainty due to irregular assessments at ICP Forests plots (minimum biweekly; Raspe et al., 2020) and flexible definitions of phenological events, affecting 1–33% of the canopy. SO is generally more difficult to estimate than spring leaf-out and remains underrepresented in phenological research (Li et al., 2023). Considerable variability in estimates has been documented both across observers (e.g. 19 days; Klosterman et al., 2014), and within populations of the same species (e.g. 19–33 days in oak, 26–28 days in beech; Delpierre et al., 2017). Due to pronounced within-canopy heterogeneity, remote sensing signals, even at 10 m resolution, primarily represent an averaged signal rather than individual tree variation. Spatial aggregation of satellite-derived SO improved agreement with field observations by reducing pixel-level noise, but at the cost of limited sensitivity to early senescence affecting only small canopy fractions. While senescence symptoms often first emerge in the sun-exposed upper canopy – which would in principle favour earlier satellite detection – earlier field-based detections likely reflect limited sensor sensitivity to low fractions of coloured foliage or litterfall, spectral mixing of senescing and non-senescing canopy elements, and signal averaging effects, consistent with the generally lower variability observed in satellite-derived SO. Overall, our results reveal a fundamental challenge in aligning categorical, observer-based ground phenology records with continuous, spatially averaged satellite-derived senescence metrics. Improving calibration of satellite-derived SO likely requires regular, objective, and species-specific reference data, such as quantifying coloured foliage fractions using high-resolution UAV imagery (Krause & Sanders, 2024) or fractional leaf area loss from weekly littertrap collections. Despite these limitations, our results showed that red-edge–based VIs such as NDRE capture SO more reliably than NDVI.

Early senescence occurrence and spatial distribution of ICP Forests plots

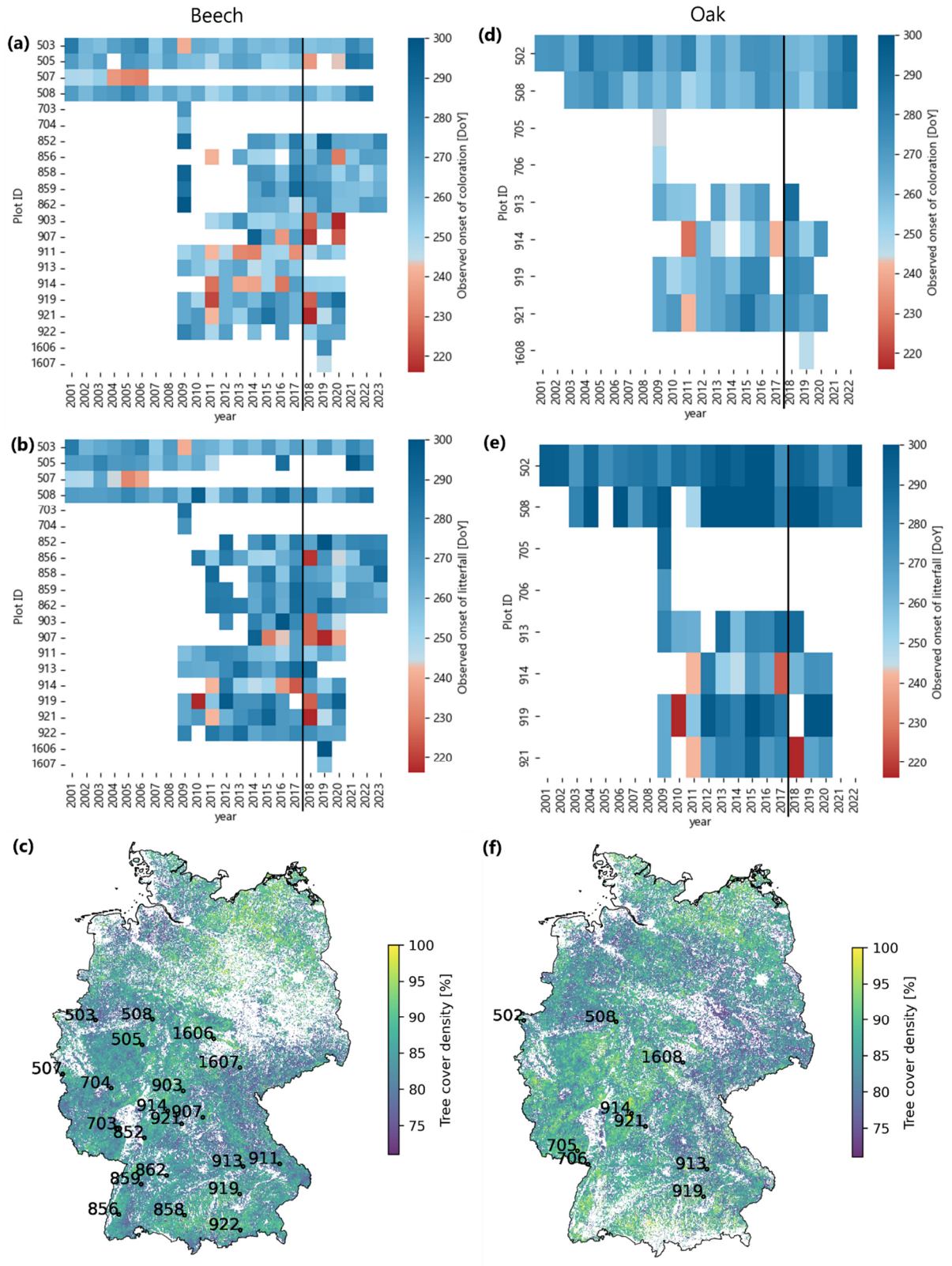

Figure S4: Interannual variability of field-observed senescence onset (SO) in beech (a-b) and oak (d-e) at ICP Forests Level II plots. Colors indicate the day of year of first observed infrequent or slight canopy coloration or litterfall (1–33% of the canopy affected). The locations of the plots with the two species are shown in subplots (c) and (f) for beech and oak, respectively. Background maps represent the average tree cover density for the species' forest pixels within each 1x1 km pixel.

Species-specific pixel counts in upscaled 1 km pixels

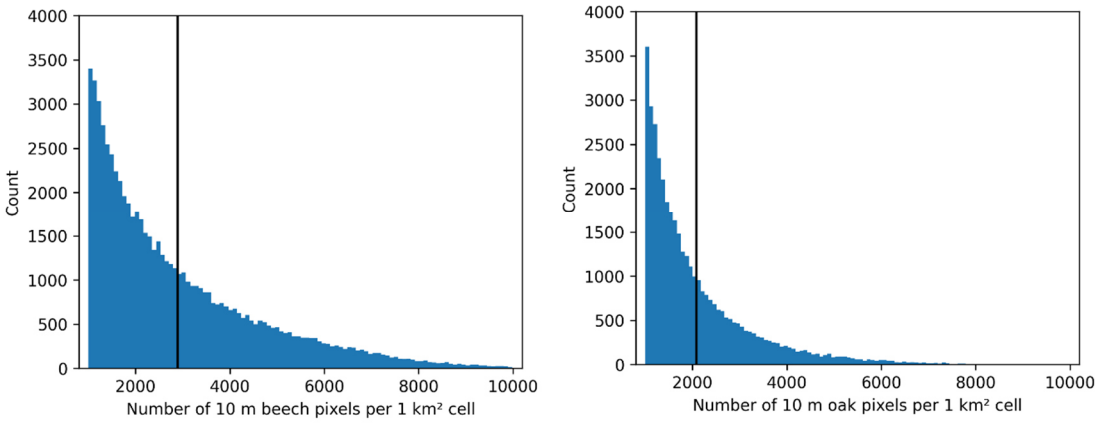

Figure S5: Distribution of the number of species-specific 10 m pixels per 1 km² grid cell after retaining only cells in which more than 10% of the cell area were covered by the respective species; i.e. beech (a) and oak (b). Vertical black lines mark the mean number of 10 m pixels per 1 km² cell.

Species-specific drought sensitivities based on standardized anomalies

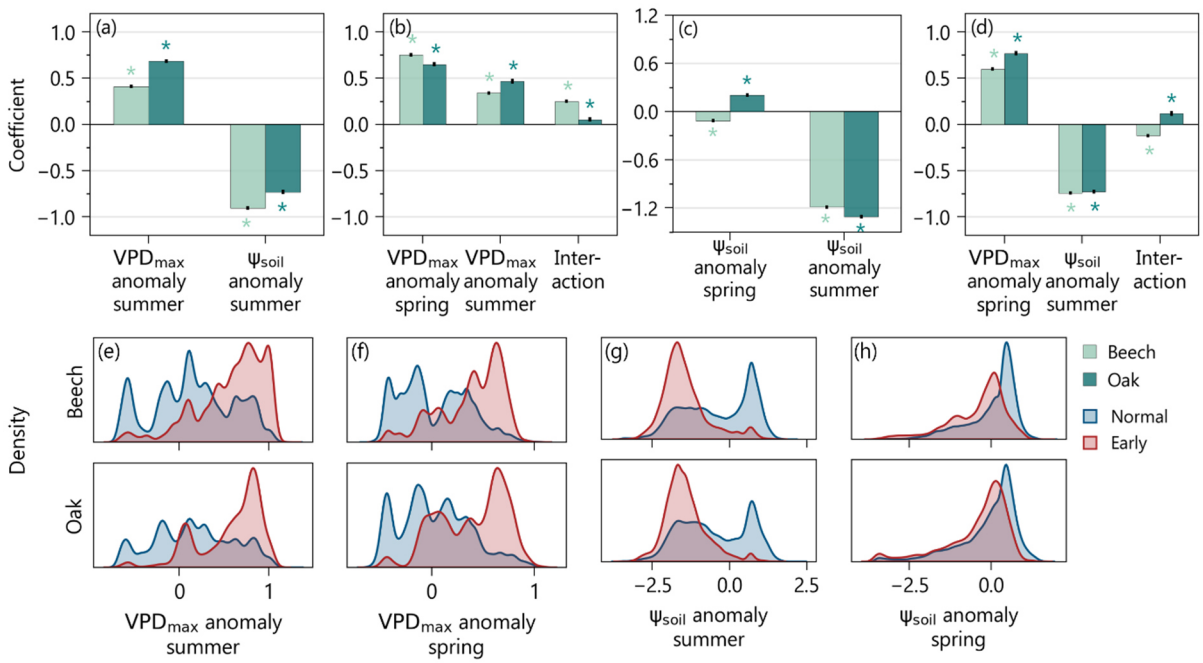

Figure S6: Different combinations of the standardized anomalies of atmospheric and soil drought stress indicators were used to explain early leaf sensecence in bivariate models. a-d) Coefficients (effect sizes) of $VPD_{max,summer}$ (1 Jul – 15 Aug) anomaly, $VPD_{max,spring}$ (15 Apr – 30 May) anomaly, $\psi_{soil,summer}$ (15–30 Aug) anomaly, $\psi_{soil,spring}$ (15 – 30 May) anomaly in four different models. Black error bars indicate the standard deviation of the coefficients across five cross-validation folds. Asterisks denote statistically significant coefficients. e-h) Probability density distributions of spring and summer VPD_{max} and ψ_{soil} anomalies for normal and early senescing forest pixels in beech (top row) and oak (bottom row).

Mortality effects 2-3 years after early senescence

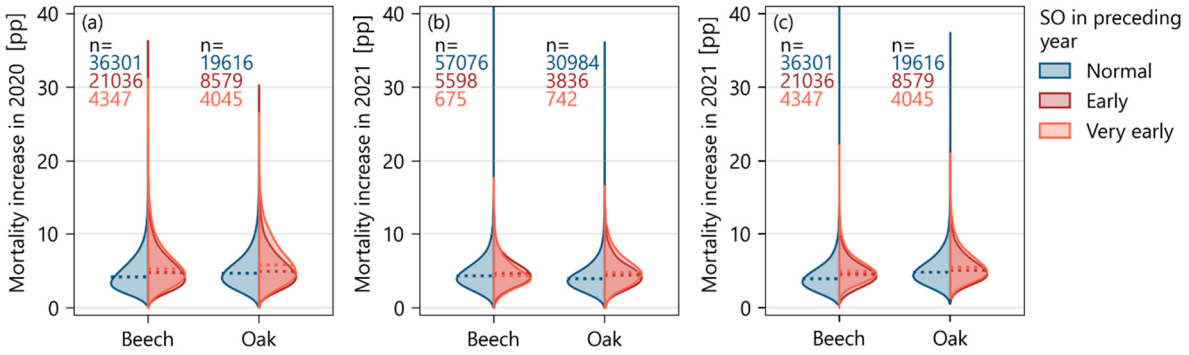

Figure S7: Canopy mortality increase (difference in fractional cover expressed in percentage points, pp) two years and three years after early leaf senescence in beech and oak forests in Germany. a) shows mortality increases in 2020 after early senescence in 2018, b) shows mortality increases in 2021 after early senescence in 2019 and c) shows mortality increases in 2021 after early senescence in 2018.

Mortality effects 1 year after early senescence

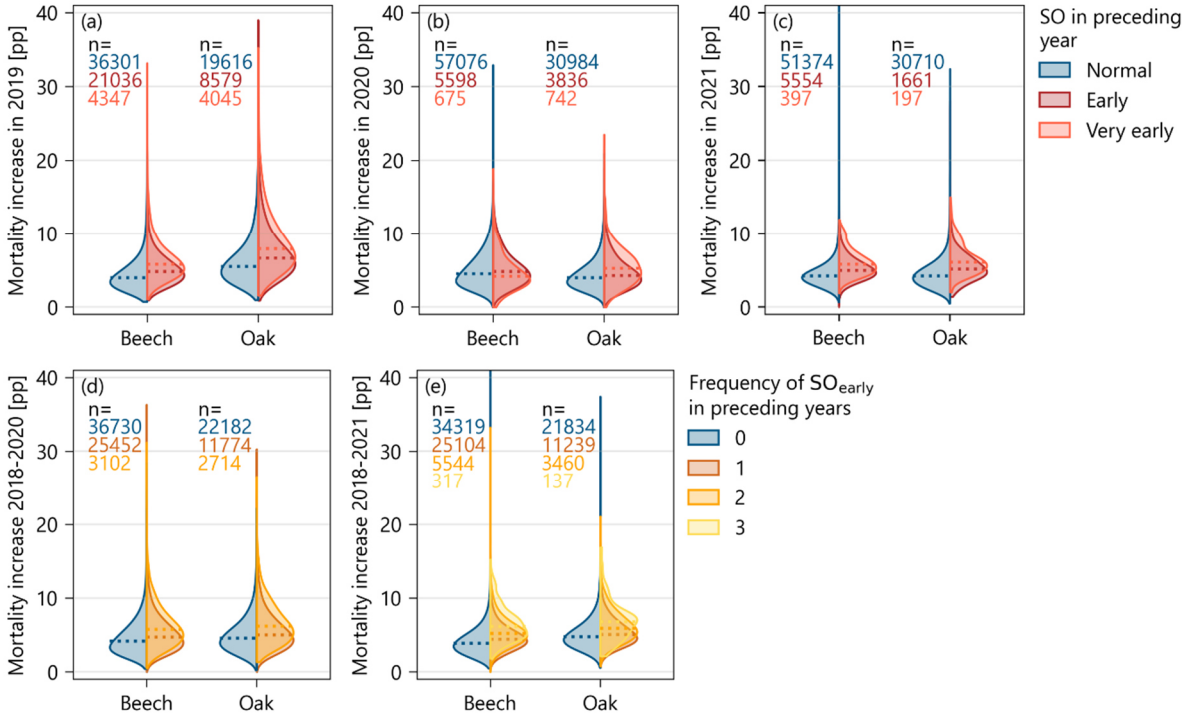

Figure S8: Mortality following early leaf senescence in beech and oak forests in Germany. a-c) Pixel-level increases in next-year canopy mortality cover in percentage points from Schiefer et al. (2023) for forest pixels with normal, early, or very early (SO before 15 August) senescence in the preceding year. Since mortality data only cover 2018-2021, the analysis is limited to the relationship between SO in 2018, 2019, and 2020 and mortality in the following year. Numbers denote sample sizes; horizontal dotted lines indicate medians of the distributions. Mortality effects beyond one year after early senescence are shown in Figure S3 (SI). d-e) Increases in canopy mortality in 2020 and 2021 (compared to 2018) after multiple early senescence events vs. no or only one occurrence in preceding years.

Vegetation indices tested

Table S1: Vegetation indices (VIs) evaluated for estimating senescence onset. Wavelength regions correspond to Sentinel-2 bands as follows: Red: B4, Rededge1: B5, Rededge2: B6, Rededge3: B7, NIR: B8.

VI	Full name	Formula	Reference
NDRE	Normalized Difference Red-Edge Index	$\frac{Rededge2 - Rededge1}{Rededge2 + Rededge1}$	(A. Gitelson & Merzlyak, 1994)
NDVIre1	Normalized Difference Vegetation Index red-edge	$\frac{NIR - Rededge1}{NIR + Rededge1}$	(A. Gitelson & Merzlyak, 1994)
CRE	Chlorophyll red-edge index	$\frac{Rededge3}{Rededge1} - 1$	(A. A. Gitelson et al., 2003)
NDVI	Normalized Difference Vegetation Index	$\frac{NIR - Red}{NIR + Red}$	(Tucker, 1979)

Environmental variables

Table S2: Environmental and site variables used in the analysis with their respective sources.

Variable	Spatial resolution	Temporal resolution	Source
Canopy cover	10 m	Single year	Copernicus Tree Cover Density 2018 (Copernicus, 2024)
Canopy height	10 m	Single year	ETH Global Canopy Height 2020 (Lang et al., 2022)
Temperature	1 km	Hourly	HOSTRADA – Hourly grids of high-resolution variables for Germany (DWD, 2024a)
CWB	1 km	Monthly	Calculated from monthly sums of evapotranspiration and precipitation (DWD, 2024b)
VPD	1 km	Hourly	Calculated from HOSTRADA temperature and dew point temperature (DWD, 2024a, 2024b)
Soil water potential	1 km	8-daily	Soil water potential in the root zone under beech and oak (P. Schmidt-Walter, personal communication, April 2025) calculated with LWF-Brook90 (Schmidt-Walter et al., 2020)
Relative extractable water	1 km	8-daily	Relative extractable water in the root zone under beech and oak (P. Schmidt-Walter, personal communication, April 2025) calculated with LWF-Brook90 (Schmidt-Walter et al., 2020)
Soil texture (sand, silt, clay fractions)	250 m	-	SoilGrids250m (Poggio et al., 2021)
Soil bulk density	250 m	-	SoilGrids250m (Poggio et al., 2021)
Soil depth	250 m	-	Soil depth in Germany / Physiologische Gründigkeit der Böden Deutschlands (BGR, 2015)
Topography	1 km	-	ASTGDEM v3 digital elevation model (Sismanidis, 2024)

Predictive performance of summer drought integration windows

*Table S3: Univariate logistic regression model performance (F1-score) depending on **different averaging time periods ending in August** for VPD_{max} and ψ_{soil}. across beech and oak forests. Numbers indicate the start and end month of the averaging periods.*

VPD_{max}		ψ_{soil}	
period	**F1-score**	**period**	**F1-score**
8_mid-8_end	0.521	6_mid-8_mid	0.510
8_start-8_mid	0.528	6_start-8_mid	0.511
6_start-8_end	0.539	7_start-8_mid	0.512
6_start-8_mid	0.541	5_mid-8_mid	0.512
5_mid-8_end	0.542	5_start-8_mid	0.512
5_mid-8_mid	0.543	4_mid-8_mid	0.513
6_mid-8_end	0.545	4_start-8_mid	0.513
6_mid-8_mid	0.551	7_mid-8_mid	0.529
8_start-8_end	0.552	6_start-8_end	0.541
5_start-8_end	0.552	6_mid-8_end	0.541
5_start-8_mid	0.554	5_mid-8_end	0.542
4_mid-8_end	0.557	5_start-8_end	0.542
7_mid-8_end	0.557	4_start-8_end	0.542
4_start-8_end	0.559	4_mid-8_end	0.542
7_start-8_end	0.560	8_start-8_mid	0.544
4_mid-8_mid	0.561	7_start-8_end	0.545
4_start-8_mid	0.563	7_mid-8_end	0.549
7_mid-8_mid	0.565	8_start-8_end	0.550
7_start-8_mid	0.567	8_mid-8_end	0.555

Predictive performance of spring drought integration windows

*Table S4: Univariate logistic regression model performance (F1-score) depending on **different averaging time periods in spring** for VPD_{max} and ψ_{soil}. across beech and oak forests. Numbers indicate the start and end month of the averaging periods.*

VPD_{max}		ψ_{soil}	
period	**F1-score**	**period**	**F1-score**
5_mid-6_end	0.445	4_mid-4_end	0.484
5_start-6_end	0.484	4_start-4_end	0.484
5_mid-6_mid	0.490	4_mid-5_mid	0.498
5_mid-5 end	0.513	4_start-5_mid	0.498
4_mid-4_end	0.522	5_mid-6_end	0.511
5_start-6_mid	0.522	5_start-6_end	0.512
5_start-5_end	0.545	4_mid-5_end	0.532
4_start-4_end	0.550	4_start-5_end	0.532
4_start-5_end	0.569	5_start-5_end	0.541
4_start-5_mid	0.570	5_start-6_mid	0.546
4_mid-5_mid	0.576	5_mid-6_mid	0.546
4_mid-5_end	0.578	5_mid-5_end	0.553

References

1. BGR, B. für G. und R. (2015). *PhysGru1000_250. Soil depth in Germany / Physiologische Gründigkeit der Böden Deutschlands* (Version 1.0) [Dataset]. https://services.bgr.de/boden/physgru
2. Copernicus. (2024). *Tree Cover Density 2018—Present (raster 10m), Europe, yearly, Nov. 2024*. Copernicus Land Monitoring Service. https://doi.org/10.2909/e677441e-fb94-431c-b4f9-304f10e4dfd8
3. Delpierre, N., Guillemot, J., Dufrêne, E., Cecchini, S., & Nicolas, M. (2017). Tree phenological ranks repeat from year to year and correlate with growth in temperate deciduous forests. *Agricultural and Forest Meteorology*, *234–235*, 1–10. https://doi.org/10.1016/j.agrformet.2016.12.008
4. DWD. (2024a). *HOSTRADA - High-resolution grids of hourly variables for Germany, Version 1.0* [Dataset]. https://opendata.dwd.de/climate_environment/CDC/grids_germany/hourly/hostrada/
5. DWD, C. D. C. (CDC). (2024b). *Grids of monthly total precipitation over Germany, version v1.0.* [Dataset]. https://opendata.dwd.de/climate_environment/CDC/grids_germany/monthly/precipitation/
6. Gitelson, A. A., Gritz †, Y., & Merzlyak, M. N. (2003). Relationships between leaf chlorophyll content and spectral reflectance and algorithms for non-destructive chlorophyll assessment in higher plant leaves. *Journal of Plant Physiology*, *160*(3), 271–282. https://doi.org/10.1078/0176-1617-00887
7. Gitelson, A., & Merzlyak, M. N. (1994). Spectral Reflectance Changes Associated with Autumn Senescence of *Aesculus hippocastanum* L. and *Acer platanoides* L. Leaves. Spectral Features and Relation to Chlorophyll Estimation. *Journal of Plant Physiology*, *143*(3), 286–292. https://doi.org/10.1016/S0176-1617(11)81633-0
8. Klosterman, S. T., Hufkens, K., Gray, J. M., Melaas, E., Sonnentag, O., Lavine, I., Mitchell, L., Norman, R., Friedl, M. A., & Richardson, A. D. (2014). Evaluating remote sensing of deciduous forest phenology at multiple spatial scales using PhenoCam imagery. *Biogeosciences*, *11*(16), 4305–4320. https://doi.org/10.5194/bg-11-4305-2014
9. Krause, S., & Sanders, T. (2024). European beech spring phenological phase prediction with UAV-derived multispectral indices and machine learning regression. *Scientific Reports*, *14*(1), 15862. https://doi.org/10.1038/s41598-024-66338-w

10. Lang, N., Jetz, W., Schindler, K., & Wegner, J. D. (2022). *A high-resolution canopy height model of the Earth* (arXiv:2204.08322). arXiv. https://doi.org/10.48550/arXiv.2204.08322
11. Li, X., Wang, X., Fang, Y., Liu, D., Huang, K., Wang, P., Zhang, J., & Yan, T. (2023). Phenology advances uniformly in spring but diverges in autumn among three temperate tree species in response to warming. *Agricultural and Forest Meteorology*, *336*, 109475. https://doi.org/10.1016/j.agrformet.2023.109475
12. Poggio, L., de Sousa, L. M., Batjes, N. H., Heuvelink, G. B. M., Kempen, B., Ribeiro, E., & Rossiter, D. (2021). SoilGrids 2.0: Producing soil information for the globe with quantified spatial uncertainty. *SOIL*, *7*(1), 217–240. https://doi.org/10.5194/soil-7-217-2021
13. Raspe, S., Fleck, S., Beuker, E., Bastrup-Birk, A., & Preuhsler, T. (2020). Part VI: Phenological Observations. Version 2020-3. In UNECE ICP Forests Programme Co-ordinating Centre (Hrsg.), *Manual on methods and criteria for harmonized sampling, assessment, monitoring and analysis of the effects of air pollution on forests.* Thünen Institute of Forest Ecosystems. https://www.icp-forests.net/fileadmin/icp_forests/Dateien/Manual_Versions/2020-22/ICP_Manual_part06_2020_Phenology_version_2020-4.pdf
14. Schmidt-Walter, P., Trotsiuk, V., Meusburger, K., Zacios, M., & Meesenburg, H. (2020). Advancing simulations of water fluxes, soil moisture and drought stress by using the LWF-Brook90 hydrological model in R. *Agricultural and Forest Meteorology*, *291*, 108023. https://doi.org/10.1016/j.agrformet.2020.108023
15. Sismanidis, P. (2024). *The ASTGDEM v3 digital elevation model for RethinkAction's Europe (EEA39) resampled at 1 km.* [Dataset]. Zenodo. https://doi.org/10.5281/zenodo.10911695
16. Tucker, C. J. (1979). Red and photographic infrared linear combinations for monitoring vegetation. *Remote Sensing of Environment*, *8*(2), 127–150. https://doi.org/10.1016/0034-4257(79)90013-0